Monitoring acoustic emission (AE) energy in slurry impingement using a new model for particle impact

M. G. Droubi, R. L. Reuben* and White, G
School of Engineering and Physical Sciences, Heriot-Watt University, Edinburgh, EH14 4AS, UK
*Corresponding author: Tel: +44 131 451 3615, e-mail: r.l.reuben@hw.ac.uk

Abstract

A series of systematic impact tests have been carried out to investigate the influence of particle size, free stream velocity, particle impact angle, and nominal particle concentration on the amount of energy dissipated in a carbon steel target using a slurry impingement erosion test rig, as indicated by the acoustic emission (AE) recorded by a sensor mounted on the back of the target. Silica sand particles of mean particle size 152.5, 231, and 362.5 μm were used for impingement on the target at angles varying between 30^o and 90^o while the free stream velocity was changed between 4.2 and 12.7 ms^{-1}.

In previous work by the authors, it was demonstrated that the AE time series associated with particle-laden air striking a carbon steel target could be described as the cumulation of individual particle arrival events each drawn from a statistical distribution model. The high arrival rate involved in a slurry jet poses challenges in resolving individual particle impact signatures in the AE record, and so the model has been extended in this paper to account for different particle carrier-fluids and to situations where arrivals cannot necessarily be resolved.

Keywords: Acoustic emission, particle impact, slurry.

1 Introduction

Slurry erosion is caused by the interaction between solid particles suspended in a liquid and a surface which experiences a loss of mass due to successive impacts of hard particles travelling at substantial velocities. Slurry erosion has been recognized as a serious problem in many industrial applications such as slurry transport pipelines, slurry handling systems and hydraulic components, causing thinning of components, surface roughening and degradation, and reduction in functional life. A number of studies [e.g. 2-4] have shown a correlation between the rate of dissipation of the kinetic energy of impact and the rate of material removal. Also, there is a general agreement that the AE energy associated with particle impingement is proportional to

the incident kinetic energy $\frac{1}{2}mv^2$ [1, 5-8]. Therefore, the measurement of AE energy associated with particle-laden liquid impingement seems likely to offer a means of monitoring slurry erosion.

There is ample experimental evidence of the effect of particle impingement parameters on erosion, and, whereas this has been reviewed in detail by the authors elsewhere [7], those studies that emphasise effects peculiar to erosion where the carrier fluid is liquid are selected here. Turenne *et al*, [9] have investigated the effect of particle concentration in a slurry on the erosion rate of aluminium samples using a narrow slurry jet of (200-300 μm) sand particles in water at normal incidence angle at a fixed velocity of 17 ms^{-1}, whilst varying the slurry concentration between 1 and 20% by weight. They characterised the so-called "blanketing effect" in dense slurries by identifying an erosion efficiency, η_e, (ratio of mass lost by erosion to mass of erodent used) which decreased with the inverse cube root of the volume fraction of sand in the stream, f:

$$\eta_e = \frac{K}{f^{0.33}}$$

where K is a constant which will depend on the erodent, the target, the jet size and the fluid velocity. On examination of the eroded surfaces, Turenne *et al* also noted that they expected that different impingement angles could result in very different effects of slurry concentration even to the extent that efficiency could increase with concentration at low angles of incidence. Fang *et al*, [10] directed a jet of silica sand (particle size 600-850 μm) suspended in water at samples of four different ceramics and found that the erosion rate did not change in a consistent way in the concentration range 3 to 7.5 wt.%, although the maximum erosion rate for all the materials investigated was at an impact angle of 90°. Iwai *et al*, [11] investigated the slurry wear rate of 13 materials and found that the effect of changing one of the experimental conditions such as jet velocity Vj, particle size d, and particle concentration C on the erosion rate of the target E_r was characterised typically by exponents whose values were chosen to fit the experimental data as follows:

$$E_r \sim V_j^{1.3-3.2}\, D^3 C^{0.5}$$

Particularly when the carrier fluid is a liquid, fluid-particle-surface interactions can have a significant effect on particle trajectories and velocities near the target, and hence on the AE energy transferred to the target. Laitone [12] was one of the first to comment that particles approaching a surface always impinge with angles of less than 90^o indicating that there is always a difference between the true incidence angle and the angle of the approaching flow. Benchaita *et al*, [13] have noted that the form and dimensions of the erosion crater in a copper target subject to a 20 mm square section jet consisting of a 0.3 wt.% suspension of silica sand in water were consistent with a spread in particle trajectories from normal to more inclined angles. They identified three regions in a jet with normal incidence; a uniform flow at the nozzle exit, a

streamlined flow near the target and a uniform exit flow parallel to the surface. In the streamlined region, the components of the flow are given by:

$$v_x = Mx \text{ and } v_y = My,$$

where x and y are measured from the stagnation point and M is a flow parameter which depends on the jet velocity, the nozzle width and the stand-off distance. These authors also noted that the boundary layer thickness, given by $\delta = 2.4\sqrt{\frac{\nu}{M}}$ (where ν is the kinematic viscosity of the fluid), relative to the particle size is important in assessing the extent to which the boundary layer will slow the impinging particles.

Clark and Burmeister [14] have identified the role of a "squeeze film" as a cushion between an approaching particle and a surface, irrespective of particle size and initial velocity of approach. They suggested that the extrusion of the intervening layer may even prevent impact entirely at low Reynolds numbers, a suggestion which was confirmed later by Wong and Clark [15] who showed that, for 50 μm glass beads in a flow at 6 ms^{-1}, impact is prevented altogether. More recently, Clark [16] has noted that knowledge of the flow conditions close to the surface in erosion testers, such as the slurry pot, is "not very sound", but that the impact velocity of particles, deduced from individual crater dimensions, can be 50% or less of the free stream velocity of the fluid. Much of this difference can be explained by potential flow taking into account the distribution of impact angles and consequent components of the velocity normal to the target, and the rest was attributed to the retardation effect of the squeeze film, with small (<100μm) particles in dense slurries being most susceptible. Not only may particles approaching the target surface at low Reynolds number be unable to penetrate the squeeze film on rebound or approach, but also, in more concentrated slurries, a layer of particles can become trapped at the surface offering the target some protection from the effect of impact by further approaching particles.

Turenne and Fiset [17] solved numerically the differential equations for particle movement in the flow field near the surface for a slurry jet impinging a surface with normal incidence. By curve-fitting their numerical results, they produced parametric equations for particle trajectories in terms of the final radial position of the particle on the surface, r, the incident speed V, and the impact angle θ as a function of initial location of the particle in the jet, r_i, the initial velocity (jet exit velocity) V_j, and the particle size d:

$$r = 0.192 d^{(-0.775 - 0.587 r_i + 0.018 v_j)} + r_i$$
$$V = -1.14 + 0.004 \frac{r_i V_j^{0.5}}{d^2} + 0.762\, d\, V_j \qquad \textbf{(1)}$$
$$\theta = \tan^{-1}(64.136\, d^{(11.094 - 7.293/r_i^{0.4} - 0.089 V_j)})$$

Turenne and Fiset noted that the predominant variable affecting the impact parameters is the particle size. Due to their higher inertia, the trajectories of larger particles are

deflected less, resulting in an impact angle closer to the original jet direction, and the impact velocity is also a higher proportion of the original jet velocity.

Monitoring of particle impact using acoustic emission (AE) relies upon a fraction of the incident kinetic energy of each impacting particle dissipating as elastic waves, which propagate through the target material before being detected by a suitably placed AE sensor. Some of the investigators in this area have concentrated on monitoring the erosion variables [18, 19], and others have concentrated on monitoring the amount of erosion [5, 20]. Acoustic Emission (AE) has been also proposed as a promising tool for on line monitoring of material removal involved in the abrasive water jet (AWJ) drilling process. For example, Mohan *et al* [21] have developed a simple physical model to determine the absorbed jet energy and correlated this with the measured energy of the AE signals at different water pressures. Kovacevic *et al* [22] also used AE to study the material removal mechanisms involved in the AWJ drilling process for three different materials. They correlated RMS AE signals with drilling depth and showed that RMS AE reduces with increase in drilling depth and attributed this to the effect of back flow of the jet which reduces the particle velocity as well as the debris present in the small diameter hole having a damping effect on the AE.

Thus, although some work has been done on correlating AE signals with wear rate, these correlations have not yet been supported with established models to offer a general, quantitative approach to predicting the energy dissipated into the material and accordingly the material removal rate using AE. The purpose of the present work was firstly to examine, over a wide range of impact conditions, the relationship between measured AE energy and a slurry jet impingement parameters, and, secondly, to extend the applicability of the statistical model described in [1] to relatively controlled impingement experiments where the carrier fluid is a liquid in order to assess the extent to which the previous findings can be applied with this medium. Emphasis is placed on the effect of fluid mechanical phenomena on the motion of particles near the target, and a free jet is used here in the interest of comparison with experiments where a free air jet has been used to accelerate particles.

2 Experimental method

The experimental set-up consisted of a slurry impingement rig and AE system with a carbon steel target assembly identical to that used for the corresponding air jet tests [1, 7]. The test rig was designed to project a jet of slurry with a controlled range of nozzle exit velocities at the target surface. The flow loop consisted of a positive displacement pump (model C22BC10RMB, Mono pump driven by a 1.1 kW geared motor to give an output speed of 587 rpm), standard 25 mm PVC piping, a 50 litre conical tank and choke valves. The slurry was first mixed by recirculating it through a by-pass leg for around 20 minutes to ensure that all the solids were suspended in the flow before diverting the flow to the nozzle as shown schematically in Figure 1.

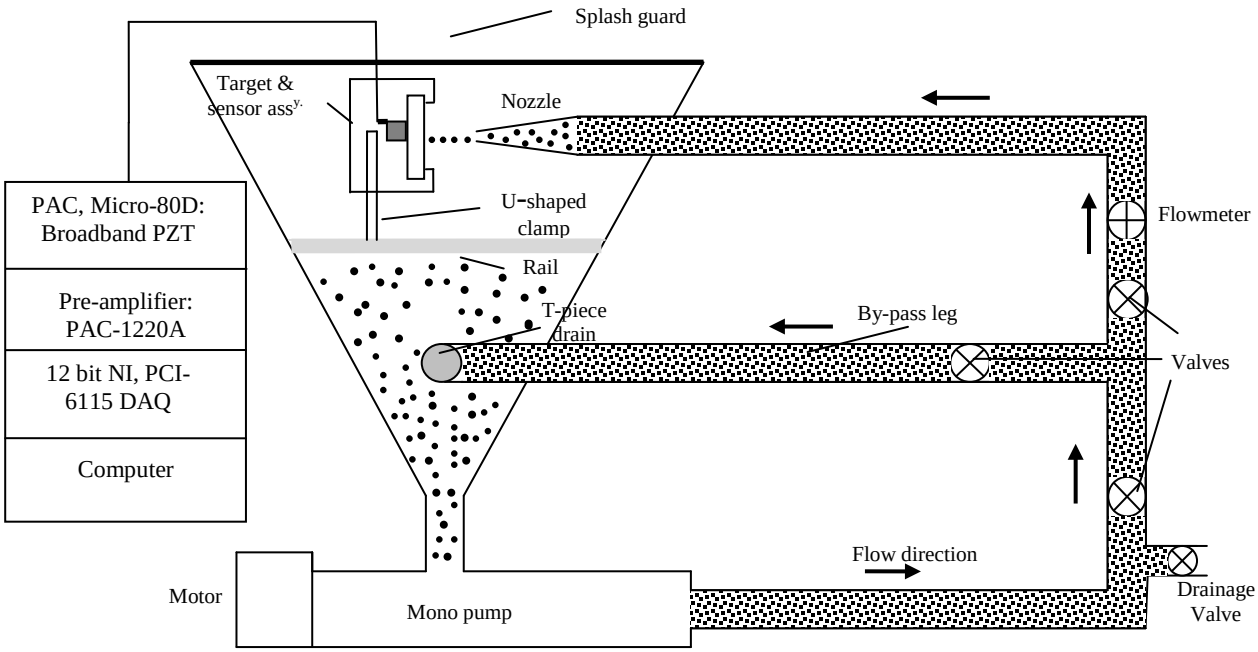

Figure 1: Experimental setup (slurry jet test apparatus) and measurement system.

The slurry stream was projected towards the specimen through a 5 mm-diameter nozzle with a 30mm stand-off distance. A broad band piezoelectric AE sensor (Micro-80D, Physical Acoustics Corp.) was coupled by means of high vacuum grease onto the centre of the rear surface of the target and then clamped onto the target. The signal from the AE sensor was pre-amplified (PAC series 1220A with switchable 20/40/60 dB gain and integral band pass filter between 0.1-1 MHz) and AE records were acquired during impingement at a sampling frequency of 2.5 MS/second for a duration of 1 second. Only the front surface of the target was exposed to the impinging slurry and great care was taken to isolate the specimen from the holder both to avoid noise and to provide reproducible results. The specimen holder was mounted onto a U-shaped clamp which was slotted to allow the slurry stream to impact the centre of the target at any pre-set angle between 0^o and 90^o. Before each test, the sensitivity of the sensor was checked by performing a pencil lead break test and, following each set of experiments where the particle size fraction needed to be changed, the test rig was drained and flushed repeatedly to remove all suspended particles.

Five 1-second records were acquired, spread evenly over a period of approximately 10 minutes, at each of three different size ranges, with each of three different impingement angles and four nozzle exit velocities, as summarised in Table 1. The size fractions were separated using a dry sieve from commercial bulk sand (Hepworth Minerals and Chemicals Ltd, UK). The particles were found to be angular with semi sharp, semi round corners, as shown in Figure 2. The mean particle masses for the graded particles were 4.8, 16.8 and 64.5 µg determined from the average diameter for each size fraction and the density of silica (2600 $kg.m^{-3}$), assuming the particles to be

spherical. The nominal concentration of the particles in the suspension was based on the amount added to the rig, but, for each combination of size fraction, nominal concentration, and jet exit velocity, the sand content of the mixture emerging from the impingement nozzle was measured by sampling the slurry jet flow at the nozzle exit. Ten samples were taken, dried in an electronic oven, and weighed to measure their sand contents, the average of these ten samples being used as the measured concentration. The launch frequency and total number of particles launched from the nozzle per second shown in Table 1 were determined by multiplying the volumetric flow rate (m^3s^{-1}) by the average measured concentration ($kg.m^{-3}$) and dividing by the average mass of a particle (kg).

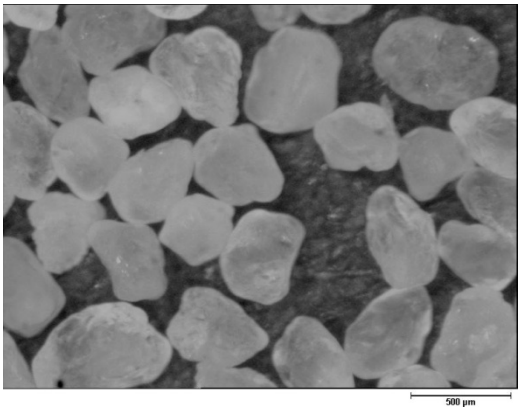

Figure 2: Silica sand erodent particles of size fraction 300-425 µm

Particle size range (μm)	Nominal concentration (kg/m^3)	Jet exit velocity (m/s)	Average measured concentration (kg/m^3)	Average launch frequency (particle/second)×10^3
125-180	10	4.2	1.6 ±0.6	27 ±41%
		6.8	5.5 ±0.8	153 ±14%
		10.2	6.1 ±1.7	254 ±29%
		12.7	1.8 ±0.7	94 ±41%
	25	4.2	11.2 ±3.5	193 ±31%
		6.8	19.5 ±1.9	543 ±9.5%
		10.2	19.8 ±0.5	791 ±3.6%
		12.7	9.6 ±1.6	490 ±17%
	50	4.2	42.5 ±2.5	736 ±6.6%
		6.8	52.5 ±4.1	1454 ±6.9%
		10.2	57.3 ±5.7	2380 ±11%
		12.7	47.2 ±2.7	2451 ±7.1%
212-250	10	4.2	1.8 ±1.4	9.2 ±76%
		6.8	6.2 ±2.1	49 ±34%
		10.2	6.2 ±2.8	74 ±44%
		12.7	5.9 ±2.6	88 ±47%
	25	4.2	10.1 ±2.9	50 ±27%
		6.8	16.4 ±0.6	130 ±8.4%
		10.2	18.4 ±1.9	220 ±11%
		12.7	14.3 ±5.2	214 ±35%
	50	4.2	42.7 ±2.3	212 ±10%
		6.8	51.3 ±2.7	408 ±5.4%
		10.2	52.9 ±6.5	631 ±16%
		12.7	54.5 ±5.6	812 ±11%
300-425	10	4.2	1.5 ±1.1	1.9 ±66%
		6.8	8.7 ±3.3	17 ±41%
		10.2	7.9 ±2.9	24 ±49%
		12.7	4.7 ±2.2	18 ±46%
	25	4.2	10.2 ±3.3	13 ±31%
		6.8	17.2 ±2.9	35 ±15%
		10.2	19.0 ±2.9	58 ±15%
		12.7	14.5 ±3.5	55 ±24%
	50	4.2	44.0 ±3.9	564 ±9.1%
		6.8	52.5 ±4.5	107 ±8.6%
		10.2	56.5 ±3.4	173 ±11.5%
		12.7	48.5 ±6.5	186 ±11.3%

Table 1: Summary of measured and derived impingement conditions

The entrainment of air into the jet and the subsequent collapse of air pockets on the target surface might generate significant AE, and so it was necessary to carry out control measurements with particle-free water to identify the background noise characteristics. Also, because the nature of the experiments might involve the removal and replacement of the sensors, it was necessary to assess the variability associated with sensor coupling to the target. Accordingly, a series of three independent runs was carried out with only water flowing, between which the sensor was removed and replaced. In each run, five AE records were taken at each of the jet exit velocities shown in Table 1. Figure 3 shows the recorded AE energy at each of the four speeds for each of the three runs. As can be seen, the variation between records for a given speed and sensor installation is negligible, while the variation between installations is slightly larger although still small in comparison with the variation with speed. The best fit power equation is also shown for each installation and, as can be seen, the exponent is about 2.5, although the fit is not particularly satisfactory, the slope increasing more rapidly at the highest speed than indicated by this exponent.

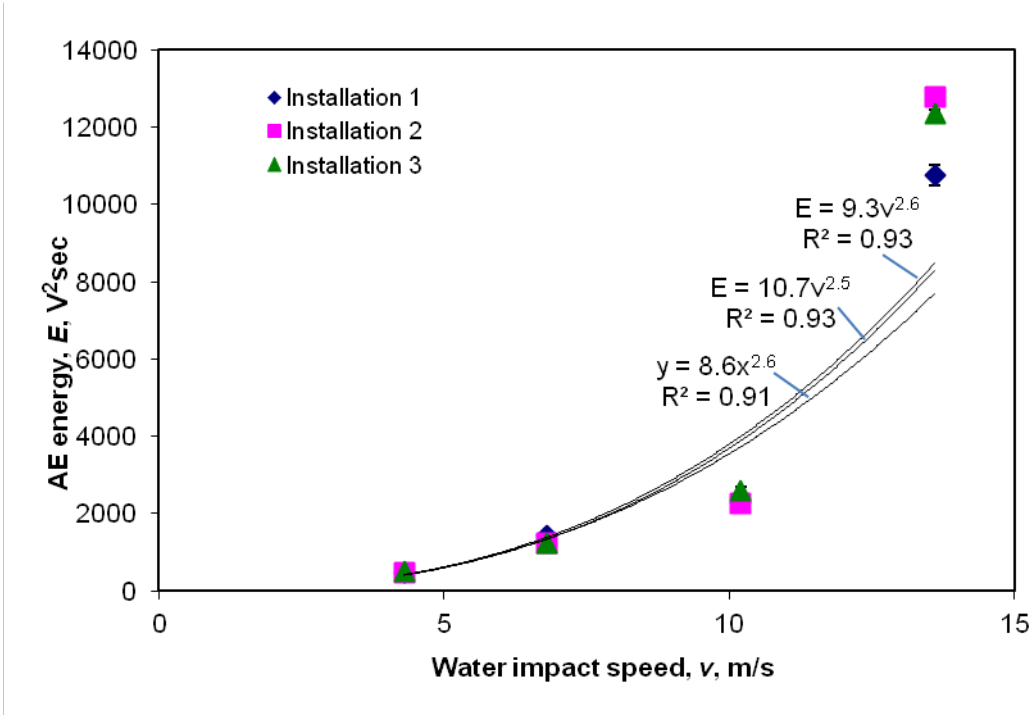

Figure 3: Recorded AE energy for pure water jet impingement

3 Results

Figure 4 shows examples of 1-second records of raw AE at the two extremes of flow speed [(i) and (ii)] without particles (a) and with the highest size fraction of particles (b). Row (c) shows segments of each of the records treated to a 100-point RMS, used in earlier work clarify particle impacts in experiments with a highly controlled particle arrival rate and energy [1]. It is clear that particles give rise to a substantial increase in AE, although the magnified views (c) do not seem to show events at the frequency

expected from the launch rates given in Table 1. This is particularly evident in Figure 4(c)(i), where only three events (of around 70 launched particles) penetrate the flow noise floor. Even at this reduced event rate, though, the higher concentration and flow speed in Figure 4(c)(ii) gives an AE signal which seems to contain a substantial amount of particle overlap.

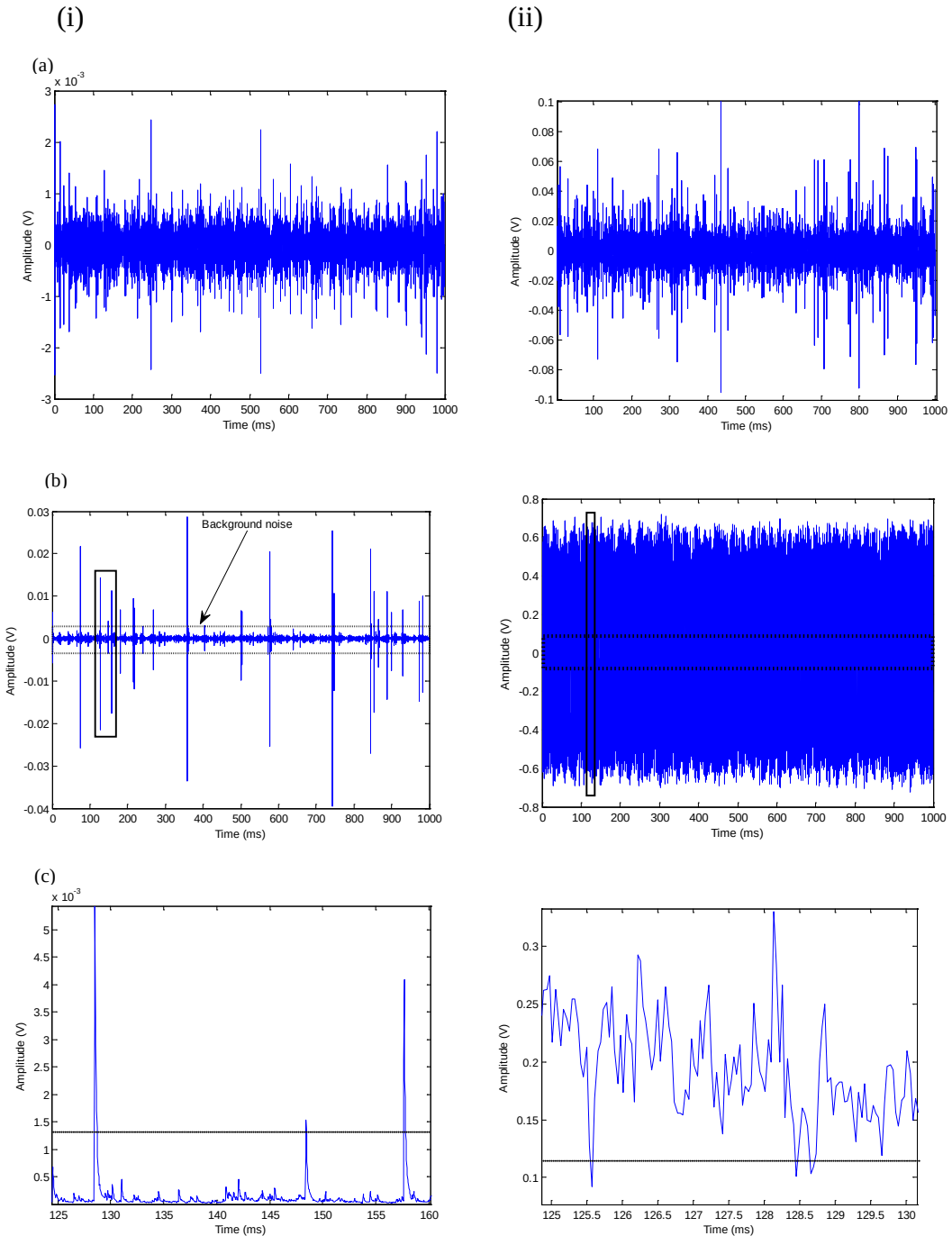

Figure 4: Typical 1-second raw AE records for **(a)** water and **(b)** slurry with 300-425 µm sand, at **(i)** a flow speed of 4.2m/s and a nominal particle concentration of 10kg/m^3 and **(ii)** a flow speed of 12.7m/s and a nominal particle concentration of 50kg/m^3 Graphs **(c)** show the 100-point RMS AE signal magnified to reveal events which penetrate the flow noise floor (dotted lines). With reference to Table 1, record

c(i) corresponds to around 70 particle launches and record **c(ii)** corresponds to around 1000 particle launches.

For each experimental condition, the measured AE impact energy was calculated from the raw signal (measured as an amplified voltage, V) by integrating over the entire record:

$$E = \int_0^t V^2(t)dt \qquad (2)$$

At least five repeat 1-second records were analysed for each condition and the average value is used in the following general analysis to establish the effects of flow speed, particle size, impact angle and concentration, against the normal expectation that energy will depend on the square of both the impact speed and the sine of the impact angle, the cube of the particle diameter (i.e. the particle mass) and will be linear with concentration, expressed as mass per unit volume of water.

Figures 5 and 6 show examples of the effect of flow speed (jet exit velocity) on the measured AE energy for a given concentration and particle size, respectively, at normal incidence. As can be seen, the error bars (corresponding to the range of the five measurements over the ten-minute period) are quite small, and the energy varies with approximately the second power of flow speed, this power dependence increasing slightly with decreasing concentration (at the particle size chosen) and appearing also to decrease slightly with decreasing particle size (at the concentration chosen). Table 2 shows the best fit power index for all of the measurements along with the associated R^2 values. The weighted average exponent calculated from $\bar{n} = \frac{\sum n_i R_i^2}{\sum R_i^2}$ was found to be 2.7, which is in reasonable agreement with other studies which report this index to lie in the range of 1.5-3 depending on the slurry properties and mechanical properties of the material under investigation [12]. It is also evident from Table 2 that exponents higher than 2 are associated with the lower concentrations where the signal:noise might be expected to be low.

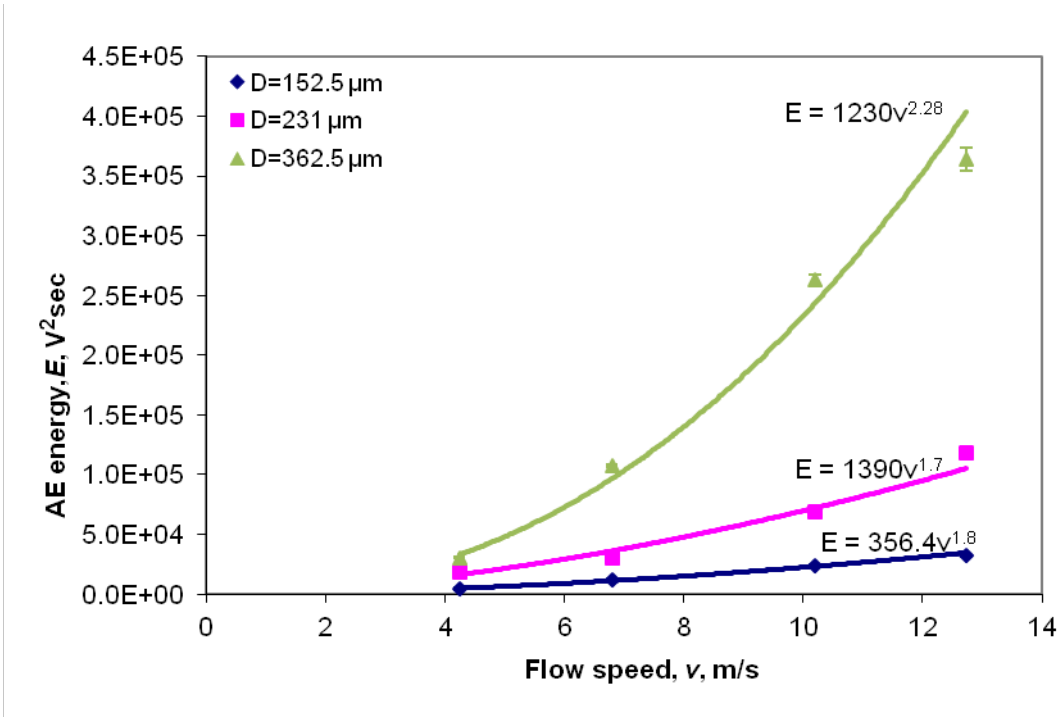

Figure 5: Effect of flow speed on AE energy for the three particle sizes at a concentration of 5kg/m^3 impinging at normal incidence.

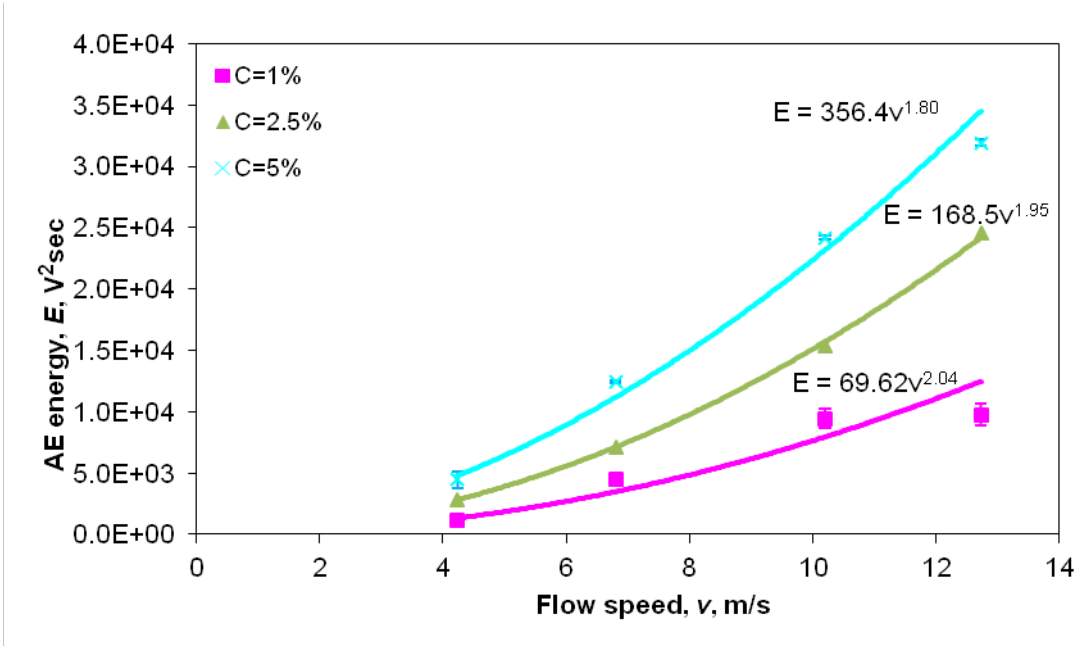

Figure 6: Effect of flow speed on AE energy for the three concentrations for particles in size range 125-180 µm impinging at normal incidence

Particle size range (μm)	Nominal impact angle θ (°)	Nominal concentration (kg/m^3)	Flow speed exponent (n)	Curve fitting R^2 value (%)
125-180	**90**	**1**	**2.0**	**94**
		2.5	**1.95**	**99**
		5	**1.8**	**98**
	60	1	3.1	78
		2.5	2.3	98
		5	1.3	99
	30	1	3.3	95
		2.5	3.3	94
		5	1.3	95
212-250	**90**	1	4.4	89
		2.5	2.2	99
		5	**1.7**	**97**
	60	1	4.3	81
		2.5	1.8	99
		5	1.8	99
	30	1	4	96
		2.5	2	99
		5	1.9	98
300-425	**90**	1	5	81
		2.5	5	91
		5	**2.2**	**99**
	60	1	5.2	93
		2.5	2	98
		5	1.8	99
	30	1	4.2	76
		2.5	2.2	99
		5	1.7	98

Table 2: Exponent of flow speed dependence of measured AE energy for all experiments. (Data in bold font are plotted in **Figures 5 and 6**)

Figures 7-9 show the effect of mean particle diameter on the measured AE energy for the range of flow speed and nominal concentration studied at normal impingement angle. Generally, the power exponent is between 2 and 3, except in the cases (low speed and lower concentrations) where there is very little particle signal (above the water “noise”) and where changes are difficult to discern at all. As for the flow speed exponent, the diameter exponent tends towards the expected value of 3 at higher concentrations whereas, at the lower speeds and concentrations, the exponent tends towards 2 (in cases where a change can be discerned). Table 3 shows the results for the remaining experiments where similar trends can be seen, leading to a weighted mean exponent of 2.1.

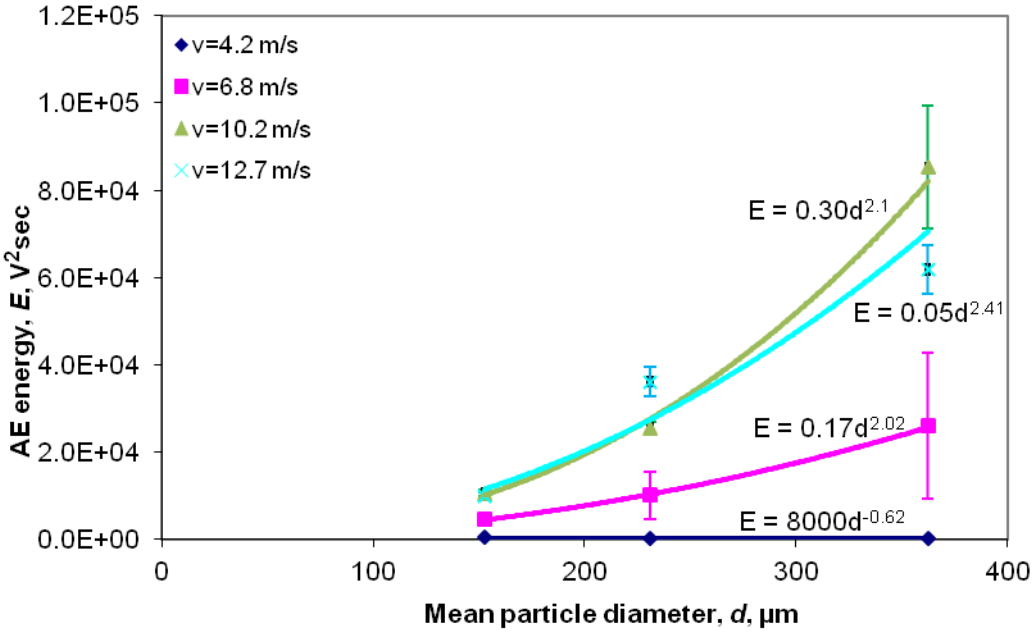

Figure 7: Effect of mean particle diameter on AE energy for normal impact at the four nozzle exit velocities with a 1% slurry.

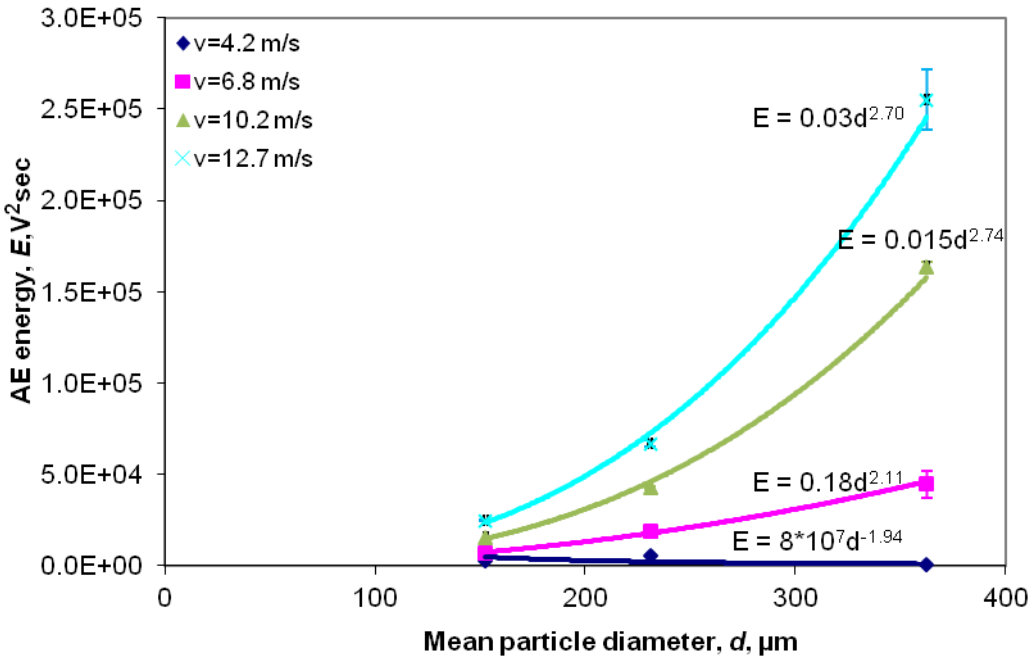

Figure 8: Effect of mean particle diameter on AE energy for normal impact at the four nozzle exit velocities with a 2.5% slurry.

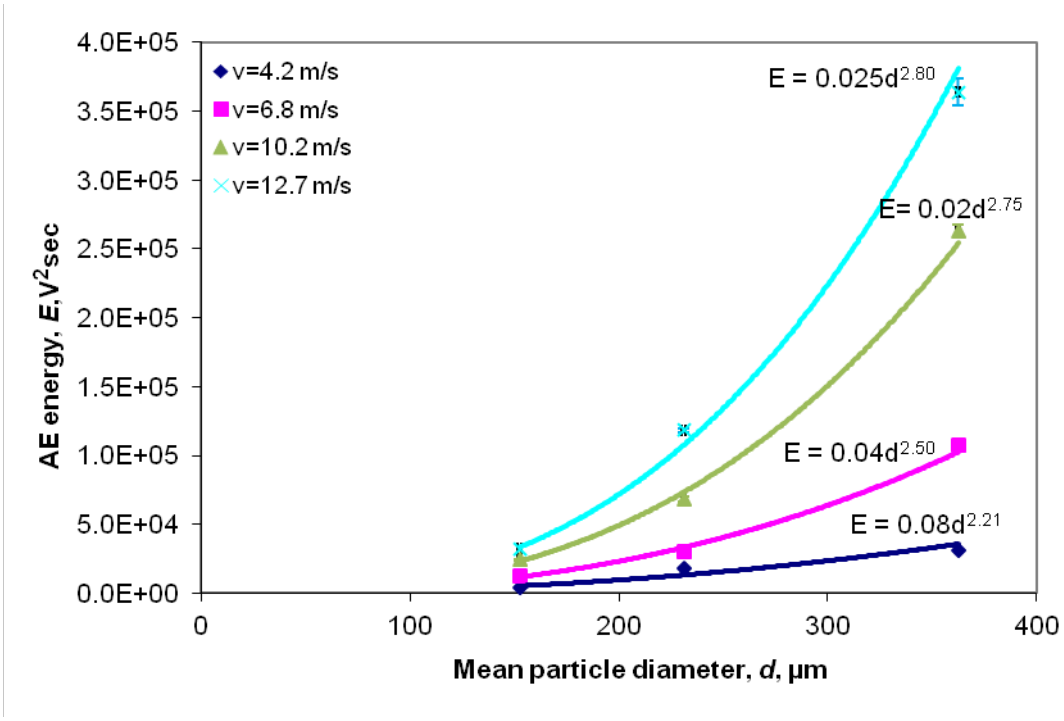

Figure 9: Effect of mean particle diameter on AE energy for normal impact at the four nozzle exit velocities with a 5% slurry.

Table 3: Exponent of particle size dependence of measured AE energy for all experiments. (Data in bold font are plotted in **Figures 7-9**)

Nominal impact angle θ (°)	Nominal concentration (kg/m^3)	Jet exit velocity (m/s)	Particle diameter exponent (m)	Curve fitting R^2 value (%)
90	**1**	**4.2**	**-**	**-**
		6.8	**2**	**99**
		10.2	**2**	**99**
		12.7	**2.4**	**93**
	2.5	**4.2**	**-**	**-**
		6.8	**2.1**	**99**
		10.2	**2.7**	**99**
		12.7	**2.7**	**99**
	5	**4.2**	**2.2**	**92**
		6.8	**2.4**	**99**
		10.2	**2.7**	**99**
		12.7	**2.8**	**99**
60	1	4.2	0.3	12
		6.8	0.5	76
		10.2	2.5	98
		12.7	2.8	98
	2.5	4.2	2.4	88
		6.8	2.2	99
		10.2	2.2	100
		12.7	2.1	97
	5	4.2	1.6	99
		6.8	1.9	100
		10.2	2.4	99
		12.7	2.2	97
30	1	4.2	-	-
		6.8	2	56
		10.2	0.7	97
		12.7	1.6	99
	2.5	4.2	3	91
		6.8	2	99
		10.2	1.7	98
		12.7	2	99
	5	4.2	2	97
		6.8	2.2	95
		10.2	2.3	88
		12.7	2.3	88

Figures 10 and 11 show the variation of the measured AE energy with nominal solid concentration for the two smaller particle size fractions and for the largest size fraction, respectively. Again, for the larger particle sizes and flow speeds, the

exponent tends towards the expected value of unity. Table 4 summarises all of the results for the concentration exponent and led to a weighted average of 1.1.

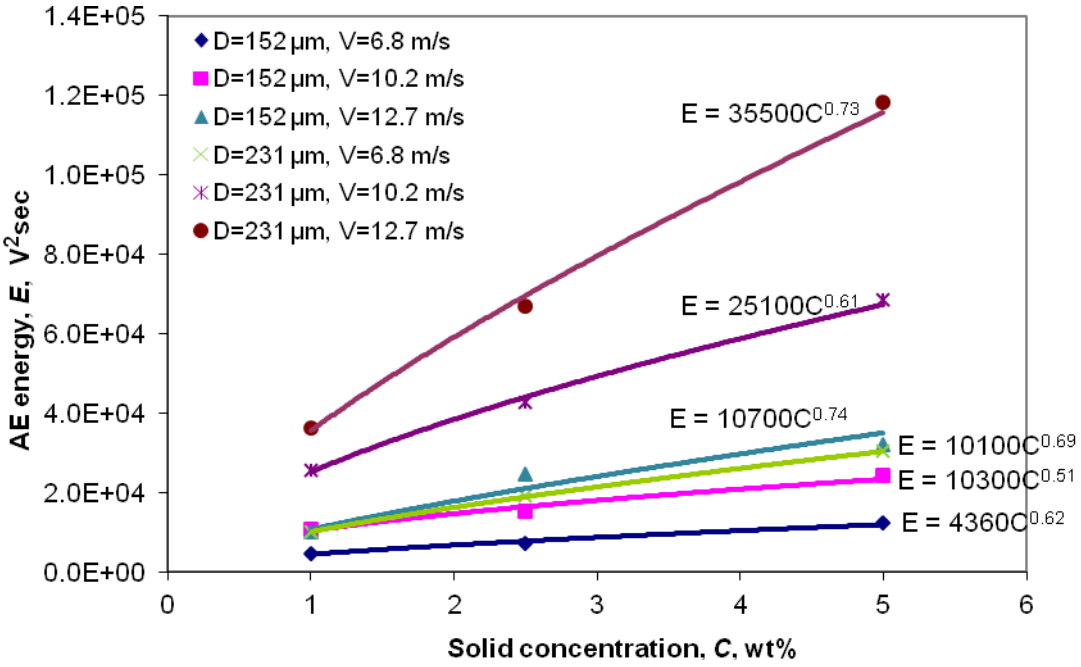

Figure 10: Effect of nominal solid concentration AE energy for normal incidence for the smaller particle sizes.

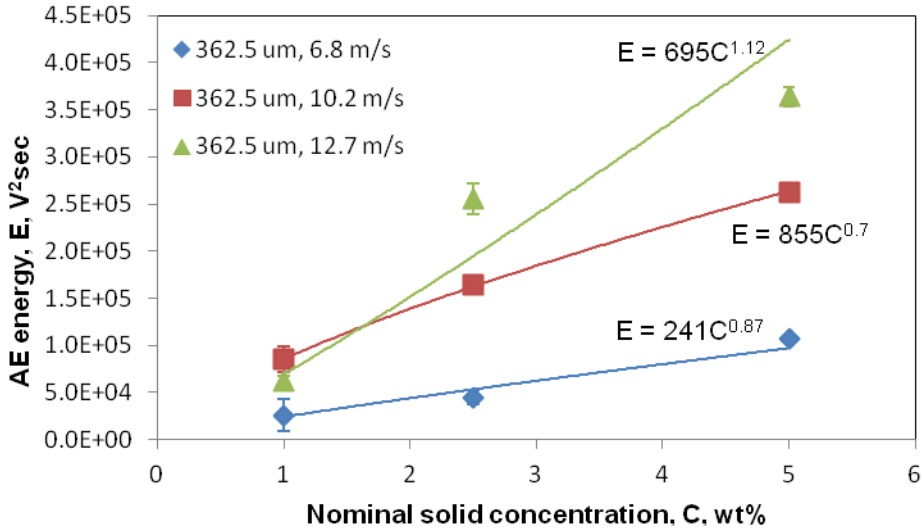

Figure 11: The effect of nominal solid concentration on AE energy, at normal incidence, for the largest particle size tested

Particle size range (μm)	Nominal impact angle θ (°)	Jet exit velocity (m/s)	Solid concentration exponent (p)	Curve fitting R^2 value (%)
125-180	**90**	4.2	1.5	0.92
		6.8	**0.6**	**0.98**
		10.2	**0.5**	**0.98**
		12.7	**0.73**	**0.94**
	60	4.2	2	0.99
		6.8	0.4	0.66
		10.2	0.5	0.97
		12.7	0.7	0.99
	30	4.2	1.6	0.79
		6.8	0.6	0.99
		10.2	0.3	0.86
		12.7	0.5	0.99
212-250	**90**	4.2	2.7	0.96
		6.8	**0.7**	**0.99**
		10.2	**0.6**	**0.99**
		12.7	**0.7**	**0.99**
	60	4.2	2.7	0.86
		6.8	0.6	0.99
		10.2	0.6	0.99
		12.7	0.9	0.98
	30	4.2	2.5	0.98
		6.8	1.6	0.98
		10.2	0.9	0.90
		12.7	1.2	0.98
300-425	**90**	4.2	2.9	0.83
		6.8	**0.9**	**0.95**
		10.2	**0.7**	**0.99**
		12.7	**1.1**	**0.93**
	60	4.2	2.8	0.91
		6.8	1.1	0.95
		10.2	0.3	0.86
		12.7	0.5	0.99
	30	4.2	3	0.95
		6.8	0.7	1.00
		10.2	0.6	0.98
		12.7	1.2	0.95

Table 4: Exponent of particle concentration dependence of measured AE energy for all experiments. (Data in bold font are plotted in **Figures 10 and 11**)

Finally, Figure 12 shows the effect of the sine of the impact angle on the measured AE energy at the highest concentration and the largest size tested and Table 5 summarises the exponents for all experiments. As can be seen, the power index occasionally approaches the expected value of 2, but there is considerable variation with no consistent pattern and the weighted average is around 1.

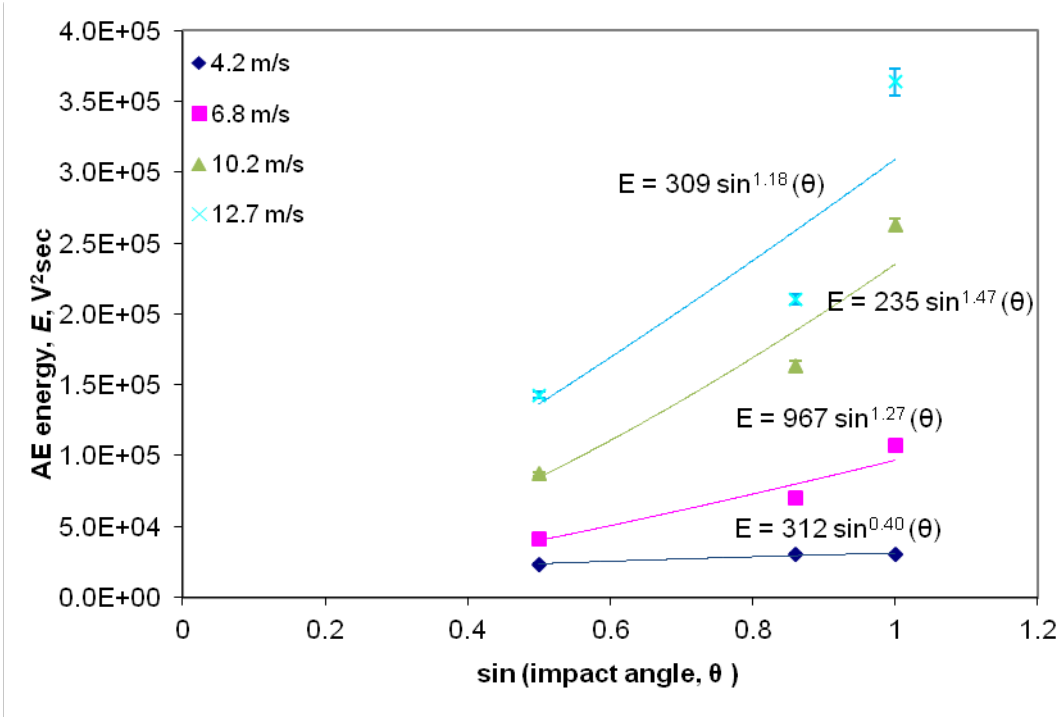

Figure 12: The effect of the sine of the impact angle on AE energy, for a 5% slurry for the largest particle size tested

Particle size range (μm)	Nominal concentration (kg/m^3)	Jet exit velocity (m/s)	Sin (impact angle) exponent (*q*)	Curve fitting R^2 value (%)
125-180	1	4.2	0.4	57
		6.8	1.1	62
		10.2	0.4	96
		12.7	0.1	29
	2.5	4.2	2.8	99
		6.8	0.77	98
		10.2	0.55	87
		12.7	0.65	94
	5	4.2	0.3	17
		6.8	1	90
		10.2	1.1	99
		12.7	0.72	96
212-250	1	4.2	0.1	8
		6.8	2.9	93
		10.2	1	99
		12.7	1.4	94
	2.5	4.2	1	55
		6.8	1	95
		10.2	1.2	97
		12.7	1.1	96
	5	4.2	0.5	68
		6.8	0.5	98
		10.2	0.22	87
		12.7	0.3	72
300-425	1	4.2	0.37	18
		6.8	0.5	21
		10.2	1.6	88
		12.7	2	82
	2.5	4.2	0	25
		6.8	0.9	93
		10.2	1.7	98
		12.7	1.4	82
	5	**4.2**	**0.4**	**97**
		6.8	**1.3**	**93**
		10.2	**1.5**	**94**
		12.7	**1.2**	**83**

Table 5: Power index for sin (nominal impact angle) dependence on the measured AE energy for all experiments. (bold text data are shown in **Figure 12**)

4. Discussion

Given that the measured energy shows roughly the expected variation with speed, particle density and particle size (although there is some doubt over the effect of jet direction), it remains to be seen whether the energy measured corresponds to what would be expected from a previously-developed log-normal distribution function which was used in [1] to describe the probability distribution of particle arrival AE energy for air-propelled particles using the same target and sensor. The mean of this distribution was found to vary with particle arrival speed in [1], and the correlation between the mean AE energy and the calculated incident energy for the dry impacts is reassessed here based on the smaller of the particle size ranges used in [1] (300-425 µm and 212-250 µm) to make the distribution compatible with the present experiments. Figure 13 shows the best fit mean along with error bars indicating the range of values over the five observations for each incident energy giving the mean AE energy:

$$mean\ p.d.f = 2.8639\ mV^2 \qquad (3)$$

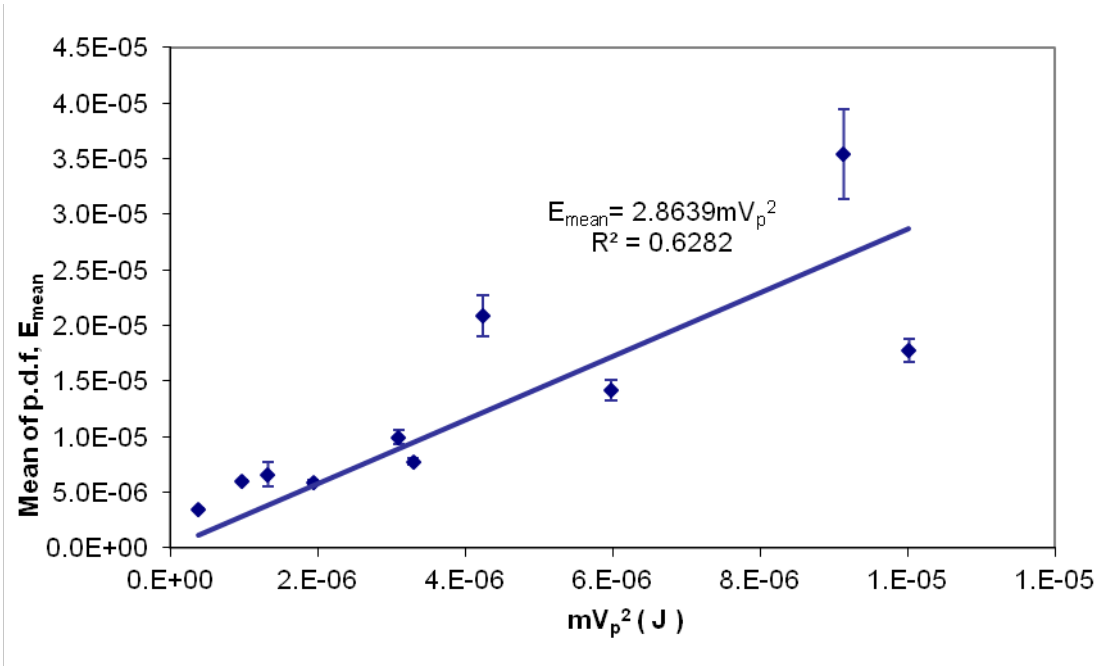

Figure 13: Correlation between the mean of the lognormal distribution and nominal incident energy for dry impacts, using data from [1].

The expected AE energy in a population of the wet impacts in this work, $E_{calculated}$, can now be obtained using the average particle arrival rate given in Table 1 and the mean of the energy distribution function:

$$E_{calculated} = mean\ p.d.f \times number\ of\ arrivals \qquad (4)$$

The measured AE energy associated with the same population of wet impacting particles, $E_{measured}$, can be estimated by subtracting the background water jet energy E_w from the integral of the signal, E:

$$E_{measured} = E - E_w \quad (5)$$

where E_w was obtained from the average of the correlation functions shown in Figure 3.

The nominal impact angle is accounted for by calculating the normal component of the jet exit velocity, and Figure 14 shows the measured and calculated energy and, as can be seen, there is a considerable discrepancy between the observed (wet) impacts and the expected energy (based on dry impacts) with the same jet exit velocity, the extension from dry impacts giving at least a factor of 10 higher AE energy.

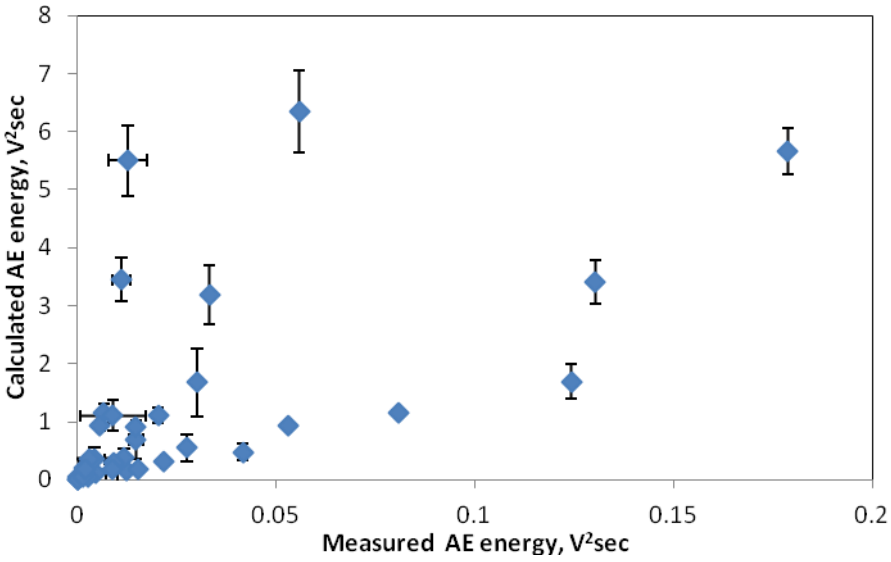

Figure 14: Measured and calculated AE energy, assuming particle arrival speeds in Table 2.

The most likely reason for this discrepancy is that particles in the wet impacts are moving much less rapidly than the jet exit velocity when they strike the target, so the empirical model (Equation 1 above) of Turrene and Fiset [17] was used to calculate the average arrival speed, using the mean particle diameter, the jet exit velocity, and taking an average value of the initial radial position of the particle (1.25mm). Table 6 shows the calculated arrival speeds for all the conditions studied. In some cases of slowly moving particles the model does not give a positive speed, corresponding to particles that fail to penetrate the squeeze film.

Both Ferrer *et al*. [8, 23] and Ukpai *et al*. [24] have published raw AE records of around 800μs duration showing impact events in slurry flows. Ferrer *et al*. [8] also made complementary measurements with single particle impacts in liquid and were able to establish a relationship between particle launch kinetic energy and AE energy, as has been done in the current work for both dry [7] and wet particle impacts. It is not

clear what impingement conditions (particle arrival rates) correspond to the record published by Ferrer *et al.* [8, 23] but there are four (possibly five) events in the 800μs, each event having a decay time of about 50μs, meaning that overlaps will occur above an arrival rate of 2×10^4 particles per second. Equally in the record published by Ukpai *et al*. [24], three impacts are shown in 600μs, each event having a decay time of about 100μs, meaning that overlaps will occur above an arrival rate of 1×10^4 particles per second. Ukpai *et al*. give the flow rate for this record as 7m/s, although they do not mention which of the three sand concentrations is relevant to the record. However, given that their minimum sand loading was 50mg/l, it is likely that the launch rate at least 1×10^5 particles per second. This would mean that these authors are achieving a similar yield (in terms of launched particles arriving at the surface) as was evident in this work. It is worth mentioning here that both Ukpai *et al*. and Ferrer *et al.* used hit-based AE systems with a threshold, meaning that they would only record the highest peaks in the time series, which may not be all of the particle arrivals.

Particle size range (μm)	Jet exit velocity (m/s)	Average calculated arrival speed (m/s)
125-180	4.2	-
	6.8	0.21
	10.2	0.73
	12.7	1.10
212-250	4.2	-
	6.8	0.30
	10.2	0.95
	12.7	1.43
300-425	4.2	0.10
	6.8	0.84
	10.2	1.80
	12.7	2.50

Table 6: Calculated particle arrival speed using the model of Turenne and Fiset [17]. Conditions indicated by a hyphen correspond to particles being unable to penetrate the squeeze film.

Figures 14 to16 show the calculated *vs* measured AE energy for each of the three impact angles, sorted for each of the particle sizes, and using the estimated impact speed following Turenne and Fiset. As can be seen, the calculated and measured values are much more compatible using this modified speed, the slope of calculated *vs* measured energy varying from a little below unity to a little above and these are listed in Table 7 along with the correlation coefficients. Figure 17 shows that the average slope is very close to unity when taking all the data together, although there is a distinct tendency for smaller particles to have higher than expected energy and larger particles to have lower than expected. Table 3 also shows the average slope to be very

close to unity for nominal impact angles of 60° and 90°, but rather less for impingement at 30°, even when the normal component is taken into account.

The particle size effect might be explained by the fact that the slurry jet is directed horizontally, so that there might be some drop-out relative to the water which would change the angle and also proportion of particles striking the surface, and this would affect larger particles more than smaller ones. Also, streams that are directed in a downward direction will have the vertical (parallel to the target) component of their velocity affected more than the horizontal, and so the lower impingement angles might be expected to have lower normal speeds than expected, and this would be expected to affect the larger particles more.

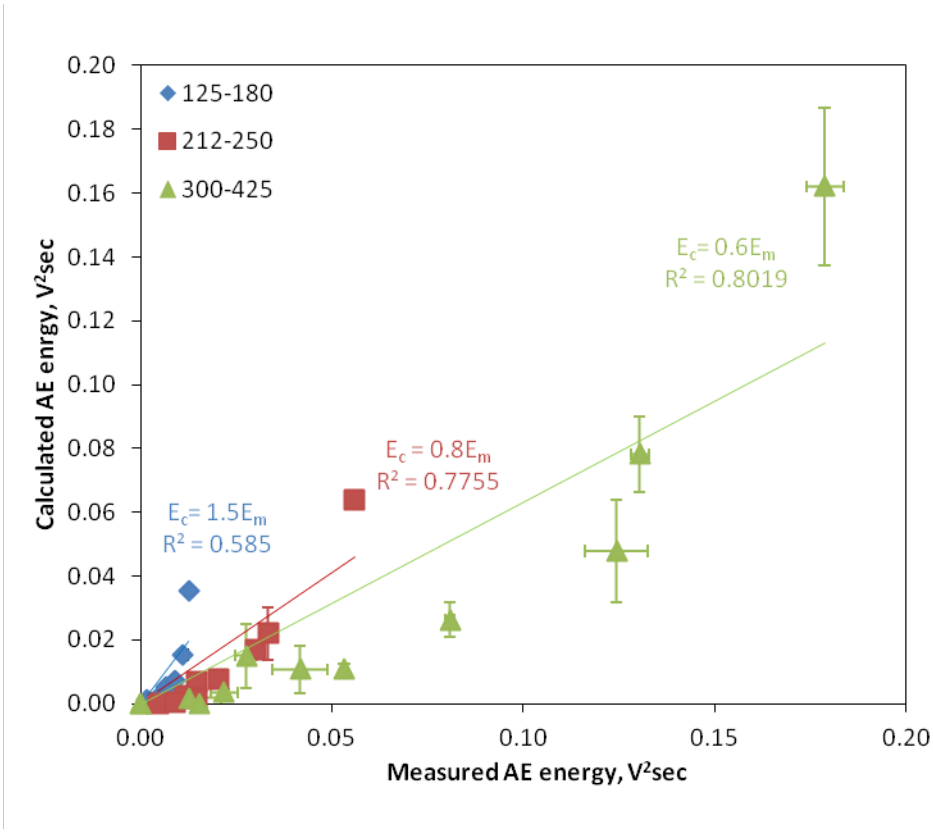

Figure 14: Calculated AE energy versus measured AE energy at nominal impact angle 90°, using modified arrival speed.

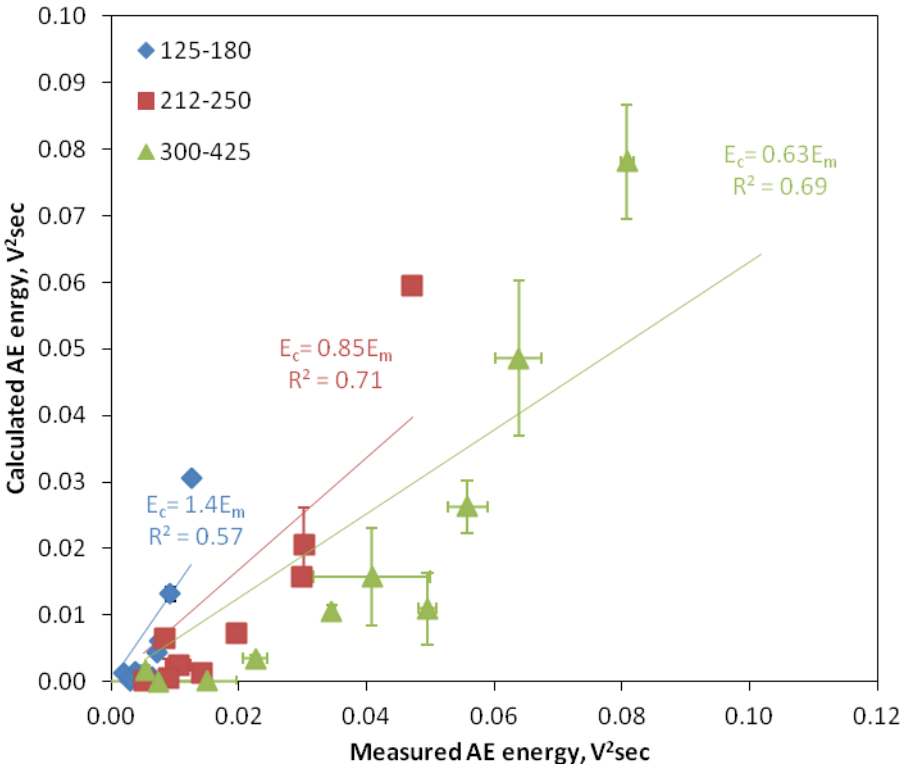

Figure 15: Calculated AE energy versus measured AE energy at nominal impact angle 60°, using modified arrival speed.

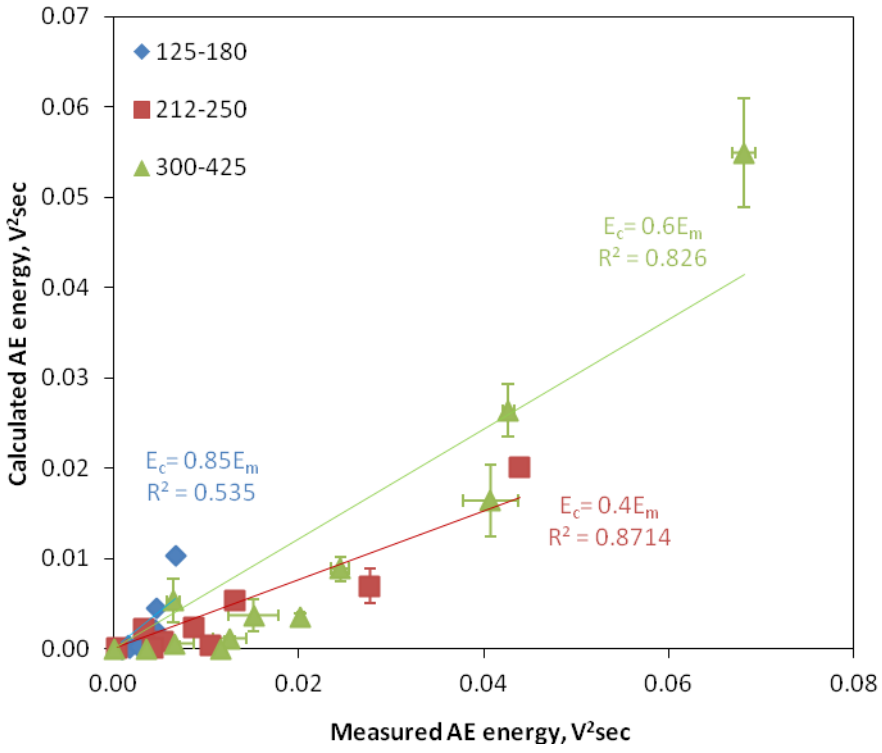

Figure 16: Calculated AE energy versus measured AE energy at nominal impact angle 30°, using modified arrival speed.

Nominal impact angle θ (^{o})	Particle size range (μm)	Slope	Correlation coefficient (%)	Average slope
90	125-180	1.53	58	0.99
	212-250	0.82	77	
	300-425	0.63	80	
60	125-180	1.39	57	0.95
	212-250	0.84	71	
	300-425	0.63	69	
30	125-180	0.83	53	0.6
	212-250	0.6	87	
	300-425	0.38	82	

Table 7: Summary of correlation functions between calculated and measured AE energy.

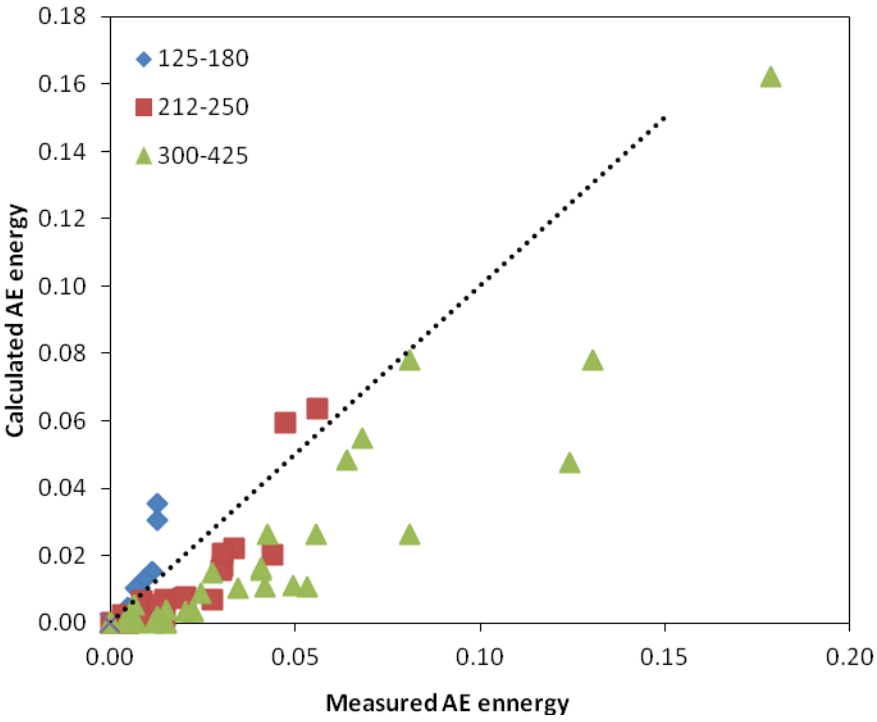

Figure 17: Calculated AE energy versus measured AE energy for all nominal impact angles investigated, using modified arrival speed.

5 Conclusions

A series of slurry impingement tests were carried out to study the effect of particle size, flow speed, particle concentration, and impact angle, on the AE energy dissipated in a carbon steel target, with the following broad findings:

1. The main problem encountered in the use of the AE technique in slurry impact experiments, compared with air-directed jets, is the high degree of particle arrival overlap and the lower-than-expected (particle) signal to (water) noise ratio.

2. The measured AE energy was found generally to scale with the expected square of velocity, cube of particle size, and linear with concentration, but with weaker expression for smaller, slower particles. The effect of jet direction was not the expected $\sin^2$ of nominal impact angle for many conditions and varied in a haphazard way around sin of nominal impact angle.

3. The cumulative impact energy, discounting that due to the water, was a factor of at least ten lower than would be expected compared with similar experiments using an air directed jet.

4. Correcting the actual arrival speed relative to the jet exit velocity using a published empirical model gave calculated cumulative energies which were much closer to those observed.

5. Larger particles tended to give lower than expected cumulative energy, an observation that is attributed to drop-out of the particles relative to the fluid in the horizontally-directed jets.

6. Lower nominal angles of impingement tended to give lower than expected cumulative energy even when the normal component of the velocity is considered. This has again been attributed to the gravitational effect on both the slurry and the particles which will affect the vertical components of the velocity relative to the horizontal one.

References

1. Droubi M G, Reuben R L and G. White, *Statistical distribution models for monitoring acoustic emission (AE) energy of abrasive particle impacts on carbon steel.* Mechanical Systems and Signal Processing, 2012, **30**, pp. 356-372.

2. Clark H M and Wong K K, *Impact angle, particle energy and mass loss in erosion by dilute slurries.* Wear, 1995, **186-187**(Part 2), pp. 454-464.

3. Tabor D, *The Hardness of Metals*, 1951, Oxford: Oxford University Press.

4. Head W J and Harr M E, *The development of a model to predict the erosion of materials by natural contaminants.* Wear, 1970, **15**(1), pp. 1-46.

5. Burstein G T and Sasaki K, *Effect of impact angle on the slurry erosion-corrosion of 304L stainless steel.* Wear, 2000, **240**(1-2), pp. 80-94.

6. Buttle D J and Scruby C B, *Characterization of particle impact by quantitative acoustic emission.* Wear, 1990, **137**(1), pp. 63-90.

7. Droubi M G, Reuben R L and White G, *Acoustic Emission (AE) monitoring of abrasive particle impacts on carbon steel.* Proceedings IMechE, Part E, Journal of Process Mechanical Engineering, 2012, **226**(3), pp. 187-204.

8. Ferrer F *et al.*, *On the potential of acoustic emission for the characterization and understanding of mechanical damaging during abrasion-corrosion processes.* Wear, 1999, **231**(1), pp. 108-115.

9. Turenne S, Fiset M and Masounave J, *Effect of sand concentration on the erosion of materials by a slurry jet*. in *Proceedings Wear of Materials - 1989*, Denver, Co., USA.

10. Fang Q *et al.*, *Erosion of ceramic materials by a sand/water slurry jet.* Wear, 1999, **224**(2), pp. 183-193.

11. Iwai Y and Nambu K, *Slurry wear properties of pump lining materials.* Wear, 1997, **210**(1-2), pp. 211-219.

12. Laitone J A, *Aerodynamic effects in the erosion process.* Wear, 1979, **56**(1), pp. 239-246.

13. Benchaita M T, Griffith P and Rabinowicz E, *Erosion of metallic plate by solid particles entrained in a liquid jet.* Trans. ASME, Journal of Engineering for Industry, 1983, **104**(3), pp. 215-222.

14. Clark, H M and Burmeister L C, *Influence of the squeeze film on particle impact velocities in erosion.* International Journal of Impact Engineering, 1992, **12**(3), pp. 415-426.

15. Wong K K and Clark H M, *A model of particle velocities and trajectories in a slurry pot erosion tester.* Wear, 1993, **160**(1), pp. 95-104.

16. Clark H M, *The influence of the squeeze film in slurry erosion.* Wear, 2004, **256**(9-10), pp. 918-926.

17. Turenne S and Fiset M, *Modeling of abrasive particle trajectories during erosion by a slurry jet.* Wear, 1993, **162-64** (pt. B), pp. 679-687.

18. Duclos, J.B., R.L. Reuben, and J.A. Steel, *A study of particle impacts in fluid flow using acoustic emission*. in *Proceedings COMADEM 2004*, Cambridge, pp. 566-575.

19. Hou R, Hunt A and Williams R A, *Acoustic monitoring of pipeline flows: particulate slurries.* Powder Technology, 1999, **106**(1-2), pp. 30-36.

20. Zhang L *et al*., *Analysis of boiler-tube erosion by the technique of acoustic emission: Part I. Mechanical erosion.* Wear, 2001, **250**(1-12), pp. 762-769.

21. Mohan R S, Momber A W and Kovacevic R, *Detection of energy absorption during abrasive water jet.* ASTME, 1995, **3**(1), pp. 69-86.

22. Kovacevic R, Kwak H S and Mohan R S, *Acoustic emission sensing as a tool for understanding the mechanisms of abrasive water jet drilling of difficult-to-machine materials.* Proceedings of the Institution of Mechanical Engineers, Part B, Journal of Engineering Manufacture, 1998, **212**(1), pp. 45-58.

23. Ferrer F et al., *A study of abrasion-corrosion of AISI 304L austenitic stainless steel in saline solution using acoustic emission technique.* NDT&E International, 2000, **33**, pp.363-371.

24. Ukpai J I et al., *Determination of particle impacts and impact energy in the erosion of X65 carbon steel using acoustic emission technique.* Tribology International, 2013, **65**, pp. 161-170.